doi: 10.46793/EEE25-1.24H

Originalni naučni rad
UDK 004.942:[536.24:697.329

Numerical Simulations of Heat Transfer in Underground Thermal Energy Storage (UTES) System: CFD Approach

Mahir Hafizović[*], Muhamed Hadžiabdić[**], Bojan Ničeno[***]

[*] Enova d.o.o. Consultants and Engineers Sarajevo, Bosnia and Herzegovina
[**] International University of Sarajevo, Bosnia and Herzegovina
[***] Paul Scherrer Institute, Switzerland

Abstract – This study presents a numerical analysis of heat transfer phenomena within an underground thermal energy storage system using Computational Fluid Dynamics (CFD). Three scenarios were analysed to examine heat transfer mechanisms: (i) *Influx of hot water* – Hot water enters the chamber, displacing colder water and transferring heat to both the surrounding soil and the outgoing water. The soil, acting as a thermal reservoir, absorbs heat with minimal temperature variation, except in regions near the chamber; (ii) *Natural cooling* – With the chamber's inlets and outlets sealed, the water gradually cools through interaction with the colder surrounding soil. The focus is on the initial cooling rate, which determines how long the water remains above a certain temperature before reaching thermal equilibrium; (iii) *Heat extraction via a heat exchanger* – A submerged heat exchanger extracts heat from the chamber water while the surrounding soil compensates for the loss. The efficiency of this process depends on the dimensions and operational parameters of the heat exchanger.
The results indicate that in all scenarios, the system maintains stable thermal stratification, with warmer water staying in the upper layers while cooler water settles due to density differences. The interaction between water and soil plays a crucial role – acting as a heat source during extraction and as a reservoir during cooling.

Index Terms – Thermal energy storage, Heat transfer, Geothermal energy, Solid-fluid interaction, Aquifer, Computational Fluid Dynamics (CFD)

I Introduction

In the global effort to mitigate climate change and reduce greenhouse gas emissions, renewable energy sources play a crucial role. However, these sources often provide energy only intermittently, as is the case with photovoltaic systems, waste heat from industrial processes, and biofuels. To overcome this limitation, it is essential to store renewable energy when available and utilize it during periods of increased demand.

Underground thermal energy storage (UTES) is a technology that stores thermal energy by heating or cooling a storage medium, enabling its use for heating and cooling applications. Aquifer thermal energy storage (ATES) is a specific type of UTES that stores heat in underground water-bearing layers (aquifers). This method, which involves the injection and extraction of water at different temperatures depending on the season, has been the subject of numerous studies [1-6], offering a viable solution for balancing energy supply and demand.

A significant challenge in ATES systems lies in accurately assessing the heat transfer rates to and from the surrounding soil. Since thermal energy is stored over extended periods – such as when water is heated during the summer months and later used for district heating in the winter – the accurate estimation of heat losses and gains from the surrounding soil becomes crucial. These estimations are necessary for evaluating the system's overall efficiency and long-term viability.

Given the complexity of heat transfer interactions between fluids and solids, along with the transient nature of these processes, numerical simulations are indispensable for predicting heat transfer dynamics with high accuracy. In systems characterized by complex geometries, convection heat transfer, significant temperature gradients, and turbulent flows, simulations that effectively resolve fluid dynamics are essential for generating reliable predictions. Computational Fluid Dynamics (CFD) is a powerful tool that enables the investigation and optimization of thermal energy storage systems. Its advantages include the ability to evaluate temperature distribution, heat transfer rates, and fluid flow patterns in a transient manner, making it particularly well-suited for analyzing ATES systems [7-10].

This study employs the CFD methodology to evaluate the heat transfer processes in various scenarios of heat storage and extraction within an ATES system, providing insights into system performance and optimization strategies.

II Considered Scenarios

Three heat transfer scenarios were systematically analysed in this study to evaluate thermal dynamics within a thermal energy storage chamber.

Scenario A examines the introduction of hot water through a pipeline into a chamber initially filled with water at the ambient temperature of the surrounding soil. As the heated water enters, it displaces the pre-existing water, which exits through a corridor at the opposite end, potentially leading to an adjacent chamber. The primary mode of heat transfer is convective, wherein the inflowing hot fluid increases the chamber temperature while the cooler fluid is displaced. Thermal conduction within the water is considered negligible. Buoyancy-driven flow significantly influences the system, particularly in the initial stages, due to

temperature gradients between the incoming and existing fluids. The soil in proximity to the chamber experiences localized heating, while the soil at greater distances remains thermally unaffected, effectively acting as a heat reservoir. Given the high thermal inertia of soil, it absorbs substantial heat without substantial temperature variations, except near the chamber boundary.

Scenario B commences from the steady-state condition achieved in Scenario A. At this stage, the chamber inlet and outlet are sealed, ceasing fluid exchange. In the absence of an external heat source, thermal dissipation occurs through conductive heat transfer to the surrounding soil, leading to a gradual decline in water temperature. Over time, thermal equilibrium is reached, where the water temperature asymptotically approaches that of the surrounding soil. The primary focus of this scenario is to quantify the transient cooling rate and assess the duration for which the water temperature remains above a prescribed threshold.

Scenario C investigates the thermal interaction between the chamber water and a submerged heat exchanger, whose external surface is maintained at a constant temperature lower than that of the surrounding water. This configuration simulates heat extraction through forced convection without direct fluid replacement. Unlike the previous scenarios, heat transfer occurs exclusively through conduction and convective exchange between the chamber water and the heat exchanger. The surrounding soil remains at an assumed fixed temperature, while the soil adjacent to the chamber undergoes thermal adjustments in response to the localized heat extraction. In this scenario, the soil functions as an effectively infinite thermal reservoir, with heat removal constrained solely by the heat exchanger's surface area and internal thermal conditions. Fluid motion is induced solely by buoyancy forces.

III METHODOLOGY

Heat transfer analysis in the chamber is conducted using the Computational Fluid Dynamics (CFD) methodology. This approach entails solving the full set of Navier-Stokes equations governing the three-dimensional motion of water, in conjunction with transport equations for energy (temperature) and turbulence properties. By employing numerical techniques, detailed distributions of velocity, pressure, temperature, and turbulent variables are obtained throughout the computational domain.

The simulations adopt a field-based approach, wherein water velocity and temperature are computed simultaneously and interactively within a time-dependent, three-dimensional framework. A computational mesh with appropriate spatial and temporal resolution is utilized to capture the time evolution of flow patterns and temperature distribution across the entire solution domain.

The numerical results enable the extraction of various averaged quantities, including time, field, and spatially averaged data. This flexibility facilitates the assessment of integral and statistical metrics such as local and average velocity, temperature, and heat flux.

The Navier-Stokes and the passive scalar transport equations in the RANS framework read:

$$\frac{\partial U_i}{\partial x_i} = 0,$$

$$\frac{DU_i}{Dt} = -\frac{1}{\rho}\frac{\partial P}{\partial x_i} + \frac{\partial}{\partial x_j}\left(\nu\left(\frac{\partial U_i}{\partial x_j} + \frac{\partial U_j}{\partial x_i}\right) - \overline{u_i u_j}\right) + g_i$$

$$\rho c_p \frac{DT}{Dt} = \frac{\partial}{\partial x_j}\left(\lambda\frac{\partial T}{\partial x_j} - \rho c_p \overline{\theta u_j}\right) + Q$$

where U_i is velocity vector, ρ is fluid density, g_i is gravity vector, ν is kinematic viscosity, T is temperature, λ is thermal conductivity, c_p is specific heat capacity, and Q is heat source.

The momentum and energy conservation equations are closed by the linear eddy-viscosity/diffusivity formulation:

$$\overline{u_i u_j} = -\nu_t S_{ij} + 2k\delta_{ij}/3, \qquad \overline{\theta u_j} = -\frac{\nu_t}{Pr_t}\frac{\partial T}{\partial x_j}$$

Where ν_t is turbulent (eddy) viscosity, and Pr_t turbulent Prandtl number set to its standard value of 0.9.

Turbulence modelling is based on the Reynolds-Averaged Navier-Stokes (RANS) approach, specifically employing the k-ε-ζ-f model by [11]. This turbulence model has been extensively validated against numerous benchmark cases, ensuring its reliability and predictive accuracy [12-17].

The ζ-f model in its original form consists of the following equations, applied also in the ensemble-averaged framework:

$$\frac{Dk}{Dt} = \mathcal{D}_k + P_k - \varepsilon$$

$$\frac{D\varepsilon}{Dt} = \mathcal{D}_\varepsilon + \frac{c_{\varepsilon 1}P_k - c_{\varepsilon 2}\varepsilon}{\tau}$$

$$\frac{D\zeta}{Dt} = \mathcal{D}_\zeta + f - \frac{\zeta}{k}P_k$$

$$L^2\nabla^2 f - f = \frac{1}{\tau}\left(c_1 + c_2'\frac{P_k}{\varepsilon}\right)\left(\zeta - \frac{2}{3}\right)$$

$$\tau = max\left[min\left(\frac{k}{\varepsilon}, \frac{0.6}{\sqrt{6}c_\mu^v|S|\zeta}\right), c_\tau\left(\frac{\nu}{\varepsilon}\right)^{1/2}\right]$$

$$L = C_L max\left[min\left(\frac{k^{\frac{3}{2}}}{\varepsilon}, \frac{k^{\frac{1}{2}}}{\sqrt{6}c_\mu^v|S|\zeta}\right), c_\eta\left(\frac{\nu^3}{\varepsilon}\right)^{\frac{1}{4}}\right]$$

$$\nu_t = c_\mu^v\,\zeta\,k\,\tau$$

where k is the RANS ensemble modelled turbulent kinetic energy, ε its dissipation rate, $P_k = \overline{u_i u_j}\frac{\partial U_i}{\partial x_j}$ is the production rate of turbulent kinetic energy, $\zeta = v^2/k$ is the velocity scale ratio, f is an elliptic relaxation function and $\mathcal{D}$ denotes the total (molecular plus turbulent) diffusion:

$$\mathcal{D}_\phi = \frac{\partial}{\partial x_k}\left[\left(\frac{\nu}{\sigma_\phi} + \frac{\nu_t}{\sigma_t}\right)\frac{\partial \Phi}{\partial x_k}\right]$$

Wall boundary conditions for all variables are prescribed within the grid cells nearest to solid surfaces, positioned beyond the viscous sub-layer. This is achieved through the application of semi-empirical wall functions, which are derived by pre-integrating the governing equations over near-wall grid cells.

The influence of surface roughness is incorporated through a

roughness model commonly employed to account for the effects of uneven surfaces or obstacles on the flow field [18].

A coupled fluid-solid simulation approach is adopted, wherein both the water and surrounding soil domains are solved simultaneously. This is facilitated through an interface that enables the exchange of heat transfer properties, such as temperature and heat flux, between the interacting domains.

The computations were conducted using the in-house finite-volume unstructured T-Flows CFD code (https://github.com/DelNov/T-Flows), developed at TU Delft by [19, 20]. T-Flows has been extensively tested and validated against multiple benchmark cases relevant to the present configurations by [12-17, 21-25].

IV Computational Details

Computational domain for Scenario A is illustrated in Figure 1. The chamber has dimensions of 200 m in length, 12 m in width, and 10 m in height. It is initially filled with 26 °C water (blue region in Figure 1) and encased by a 3 m thick soil layer. Hot water (red stream in Figure 1), with an inlet temperature of 70 °C and a velocity of 1 m/s, enters through a 0.3 m diameter opening located at the ceiling of the chamber's left end. This opening represents the exit of a pipe extending from the earth's surface. The centre of the inlet is positioned at the mid-width of the chamber and 6 m from the left wall. Under these conditions, the inlet water mass flow rate is 72.2 kg/s, equivalent to 254.3 m^3/h. The water exits the chamber through a 3 m × 3 m opening at the chamber's bottom, located diametrically opposite the inlet. The water is initially motionless. The chamber walls are assumed to be rough to replicate the natural unevenness of the surface, with a roughness coefficient of 0.05 m.

The nominal inlet power is determined based on the temperature difference between the incoming and initial water temperatures, calculated as follows:

$$\dot{Q}_{nom} = \dot{m} c_p (T_{in} - T_{ref}) = \ 12.7 \text{ MW}$$

where $\dot{Q}_{nom}$ is the power supplied, c_p is the specific heat for saline water, T_{in} is the inlet water temperature, T_{ref} is the initial temperature, and $\dot{m}$ is the incoming mass flow rate.

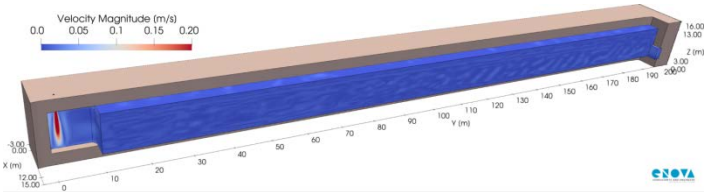

Figure 1. Cross-section of the computational domain for Scenario A

The computational domain for Scenario B is identical to that of Scenario A, except that no inlets or outlets are present, preventing any exchange of water with the surroundings.

The computational domain for Scenario C, illustrated in Figure 2, corresponds to those of Scenarios A and B. However, Scenario C also lacks any inlets or outlets for water flow, with the addition of a submerged heat exchanger within the chamber. The heat exchanger is modelled as a vertically oriented cylinder (yellow cylinder located in the middle of the chamber, Figure 2) with a diameter of 0.3 m, extending from the chamber's ceiling. Positioned 5 m below the chamber's mid-height, its centre is aligned with the chamber's midpoint. The surface area of the heat exchanger is 4.78 m^2, and its surface temperature is maintained at a constant value. Computations are conducted for five different heat exchanger wall temperatures, varying from 16°C to 24°C in increments of 2°C.

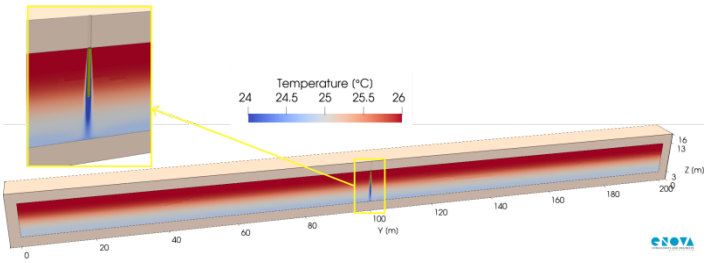

Figure 2. Cross-section of the computational domain for Scenario C

The computational mesh, illustrated in Figure 3, remains consistent across all scenarios. The blue grid covers the fluid domain, while the green grid covers the solid domain. The mesh comprises approximately 8×10^5 computational cells, with 5×10^5 cells allocated for discretizing the solid domain and the remaining cells used for fluid domain discretization. The average cell size within the fluid domain is 1 m × 1 m in the horizontal directions, while the maximum cell size in the vertical direction is 0.5 m. The mesh is refined near all walls, including the interface between the fluid and solid domains, ensuring that the distance between the wall/interface and the first cell centre is 0.004 m. The mesh consists exclusively of hexahedral cells, which are preferred due to their superior numerical accuracy and stability. The temporal resolution is set to two seconds.

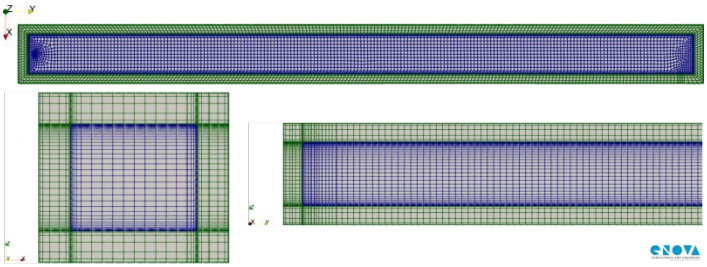

Figure 3. Top, front, and side views of the computational mesh used in simulations

V Results and Analysis

Scenario A: Influx of hot water

The heating of the water inside the chamber, initially at rest, is simulated over a period of 23 days, during which hot water enters through an opening at the chamber's ceiling. At the end of this period, both the mean water temperature within the chamber and the temperature of the exiting water converge to a common value, indicating that the statistically steady state has been reached.

Figure 4 presents the distribution of the velocity component in the Y direction, corresponding to the predominant horizontal velocity from the inlet to the outlet, in the mid-plane after 23 days of simulation. The results reveal the formation of distinct flow layers within the chamber. Near the ceiling, water exhibits rightward motion, whereas a counterflow to the left is observed in the layer beneath. Near the chamber floor, the flow direction again shifts to the right. The magnitude of the velocity component in the Y direction remains below 0.03 m/s throughout the chamber.

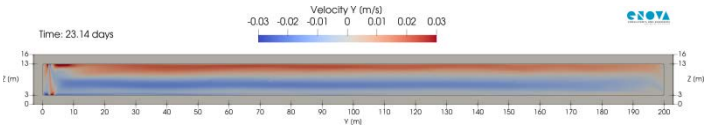

Figure 4. Velocity field of the Y-component in the mid-plane after 23 days of simulation for Scenario A. The positive Y direction is oriented to the right. Red shades indicate water motion to the right, while blue shades represent flow to the left

Figure 5 presents the temperature field in the mid-plane after 23 days of simulation. As hot water enters the chamber, it rises toward the ceiling, while cold water remains near the bottom due to buoyancy effects driven by density differences. This leads to a system exhibiting stable thermal stratification. In the upper portion of the chamber, the water shows weak stratification, approaching near-isothermal conditions, whereas strong stratification is observed near the bottom wall. This distinction is clearly reflected in the temperature profile along a vertical line through the chamber's midpoint, as shown in Figure 6, which illustrates the temperature variation from the bottom to the top of the chamber.

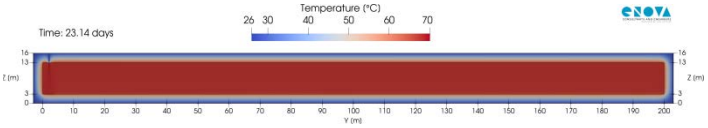

Figure 5. Temperature field after 23 days of simulation in mid-plane for scenario A

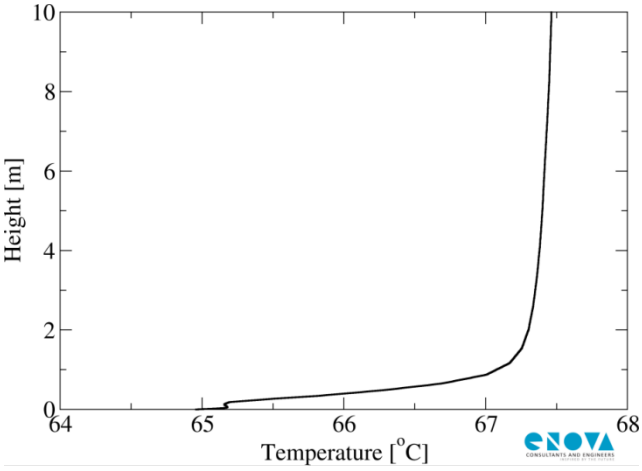

Figure 6. Temperature profile along a vertical line at the midpoint of the chamber

The water temperature exhibits spatial variations, and due to continuous cooling from the soil, the system never reaches an isothermal state. Thermal stratification persists as a result of buoyancy forces. However, the average water temperature within the chamber and the average temperature of the outflow can be determined. These profiles are presented in Figure 7 (left). Initially, during the first 3-4 days of hot water injection, the average water temperature increases rapidly in a linear manner. Thereafter, the rate of increase slows, following a logarithmic trend where temperature gains diminish over time. The profiles eventually converge at 67.4°C, which is reached after approximately 20 days.

The average heat flux at the water-soil interface is shown in Figure 7 (right). At the beginning, the heat flux rises as the temperature difference between water and soil increases due to the influx of hot water. However, after 3-4 days, as the rate of water temperature rise slows and the surrounding soil begins to warm, the temperature difference decreases, leading to a gradual decline in heat flux. After approximately 20 days, the heat flux stabilizes at around 65 W/m².

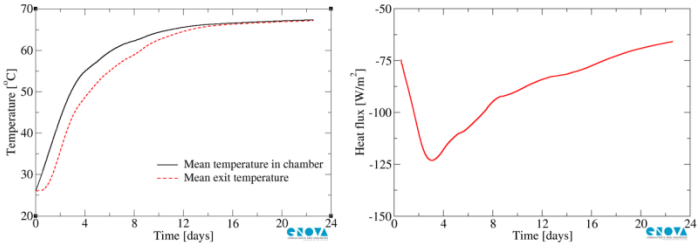

Figure 7. (Left) Time evolution of the average water temperature in the chamber and the exit water temperature (Right) Time evolution of the average heat flux at the water–soil interface

The relationship between the temperature difference (ΔT) and heat flux is well established, as heat flux is a direct function of ΔT. However, instead of relying solely on heat flux, a more insightful and universal approach is to estimate the heat transfer coefficient, *h*, as follows:

$$h = \frac{\dot{q}}{T_{in} - T_{wall}}$$

where $\dot{q}$ represents the heat flux, T_{in} is the inlet water temperature, and T_{wall} is the cavity wall temperature. From our simulations, the obtained heat transfer coefficient h is 1.48 W/m²°C. This provides a straightforward method for calculating the heat flux for different inlet temperatures. For instance, with an inlet temperature of 80°C, the heat flux would be:

$$\dot{q} = h(T_{in} - T_{wall}) = 1.48 \cdot (80 - 26) = 79.9\ W/m^2$$

Unlike heat flux, which varies proportionally with ΔT, the coefficient h depends primarily on factors such as fluid velocity, surface geometry (e.g., flat, cylindrical, spherical, or curved), fluid properties, and surface roughness. Importantly, these parameters remain relatively constant within the dimensions of the cavity under consideration. Consequently, as long as the system involves a cavity with flat walls, fluid velocities on the order of 1 m/s (approximately 0.5–10 m/s), and temperatures ranging from 20°C to 90°C, the heat transfer coefficient can be considered universal. Furthermore, within this temperature range,

the thermophysical properties of water do not change significantly enough to impact heat transfer behaviour. The obtained value of *h* remains consistent under these conditions, providing a reliable means to calculate heat flux for different inlet temperatures in a straightforward manner.

Scenario B: Natural cooling

This scenario, a continuation of Scenario A, involves sealing the chamber's inlet and outlet, preventing water exchange. Consequently, the hot water inside the chamber cools solely through heat transfer to the surrounding soil. The simulated cooling period in this scenario is approximately 41 days.

Figure 8 presents the temperature distribution after 41 days of simulation. Stable thermal stratification is observed, with cooled water accumulating at the bottom of the chamber. Initially, a temperature gradient is evident only within the lower 2 meters, while the remaining chamber remains nearly isothermal. Over time, colder water gradually infiltrates the isothermal region, leading to a more diffuse temperature gradient, as illustrated in Figure 9.

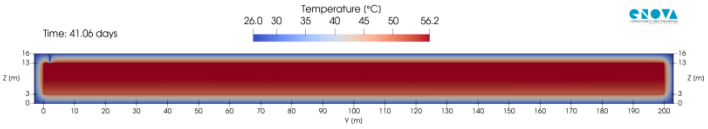

Figure 8. Temperature field after 41 days of simulation in mid-plane for scenario B

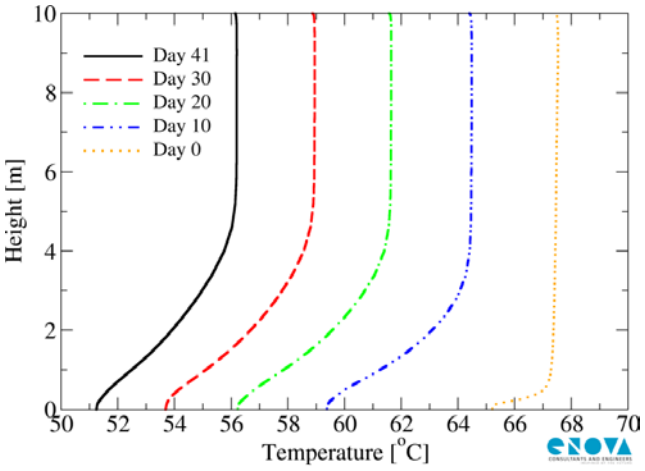

Figure 9. Temperature profiles along a vertical line at the chamber's center at different time instances

Figure 10 illustrates the average water temperature in the chamber during the natural cooling scenario. Over 41 days of simulation, the average temperature decreases from 67.4°C to 55.3°C, corresponding to an average cooling rate of 0.295°C per day. In a worst-case scenario, assuming a linear temperature decline, the water would reach 30°C in 127 days and 26°C in 140 days. However, due to the nonlinear nature of heat transfer, the actual cooling process deviates from a linear trend, resulting in prolonged heat retention. A more accurate prediction of the cooling rate can be obtained using an exponential function of the form:

$$T = Ae^{b \cdot t} + C$$

where *T* is the predicted water temperature in °C, *t* is time in days, and constants *A*, *b* and *C* are given in Table 1. According to the given exponential relation, the temperature of the water is expected to reach a value of 30 °C in approximately 274 days.

Table 1. Coefficients for exponential temperature prediction

A	b	C
41.17	-8.449×10^{-3}	26.00

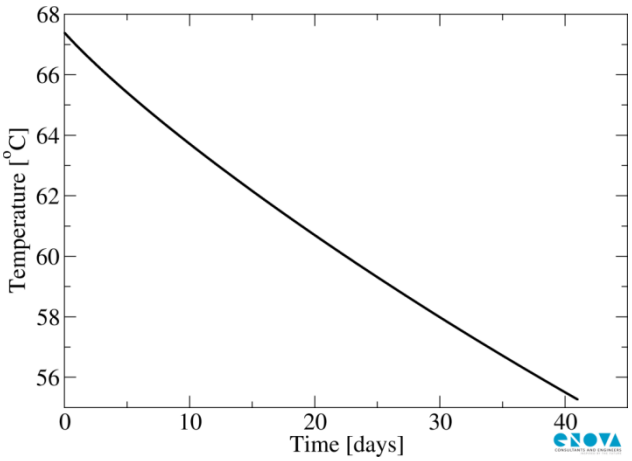

Figure 10. Time evolution of the average water temperature in the chamber during Scenario B

Scenario C: Heat exchanger

In the third scenario, heat extraction from the chamber is facilitated by a heat exchanger. The key parameter in this case is the amount of thermal energy that can be extracted, which is determined by the heat flux at the heat exchanger surface.

Figure 11 presents the velocity magnitude field in the mid-plane of the chamber after 5 days of computation, assuming a 10°C temperature difference between the heat exchanger surface and the chamber water. The highest velocity, 0.13 m/s, occurs beneath the heat exchanger. As water contacts the heat exchanger, it cools below the surrounding water temperature and descends toward the chamber bottom. Upon reaching the bottom surface, the cooled water spreads radially at a significantly lower velocity.

Figure 12 illustrates the temperature field in the mid-plane after 5 days of computation, considering the same 10°C temperature difference. A weak but stable thermal stratification is observed, with cooler water accumulating at the bottom and warmer water remaining at the top. As the cold water reaches the chamber's bottom, the surrounding soil acts as a heat source, transferring thermal energy back to the water.

Another computation was conducted for a scenario in which the temperature difference between the heat exchanger walls and the initial water temperature was set to 16°C. The water in the chamber was initially at 26°C, while the heat exchanger walls were maintained at 10°C. Over an extended period, the system evolved toward a steady-state equilibrium, where the final

temperature of both the water and heat exchanger walls stabilized at 15°C. The initial heat flux at the heat exchanger surface was 120,000 W/m^2, but as equilibrium was approached, it gradually decreased to 28,000 W/m^2. Throughout this process, the surrounding soil acted as a thermal energy source, supplying heat to the water that was extracted by the heat exchanger. Once steady-state conditions were reached, the heat flux supplied by the soil to the water stabilized at 14 W/m^2. Additionally, the temperature of the chamber walls, which initially matched the water temperature at 26°C, gradually decreased to 16°C as thermal equilibrium was established.

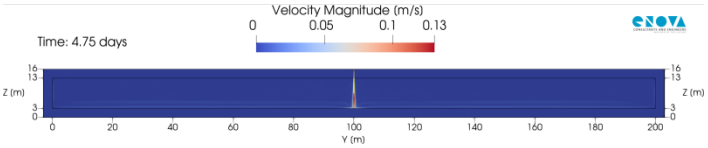

Figure 11. Velocity magnitude field after 5 days of computation in the mid-plane for Scenario C, with a 10°C temperature difference

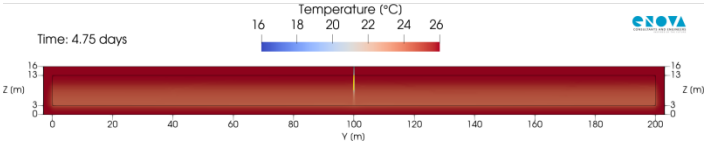

Figure 12. Temperature field after 5 days of computation in the mid-plane for Scenario C, with a 10°C temperature difference

Numerical computations have been performed for five different values of ΔT, representing the temperature difference between the heat exchanger surface and the water temperature in the chamber. Table 2 summarizes the heat flux values obtained numerically, along with their corresponding temperature differences.

Table 2. Heat flux at the heat exchanger surface for the corresponding temperature difference

ΔT [°C]	2	4	6	8	10
Heat flux q [kW/m^2]	1.921	9.231	27.611	43.784	62.126

As expected, the heat flux increases with the temperature difference, indicating that larger temperature differences facilitate the extraction of greater amounts of energy from the water in the chamber. However, this increase is not linear. The data suggests that the relationship follows power-law dependence. Based on the data in Table 2, the power law can be expressed as:

$$q = A \cdot \Delta T^B$$

where $q\ [kW/m^2]$ is the heat flux, $\Delta T\ [°C]$ is the temperature difference, $A = 0.43808$, and $B = 2.2087$. The power law approximation is plotted against numerical computations results in Figure 13.

Given the value of the heat exchanger's area, the amount of power that can be extracted using the heat exchanger can be calculated as follows:

$$Q = q \times A_{HE}$$

where $Q\ [kW]$ is total energy extracted, $q\ [kW/m^2]$ is heat flux at heat exchanger's surface, and $A_{HE}\ [m^2]$ is the area of the heat exchanger in contact with water.

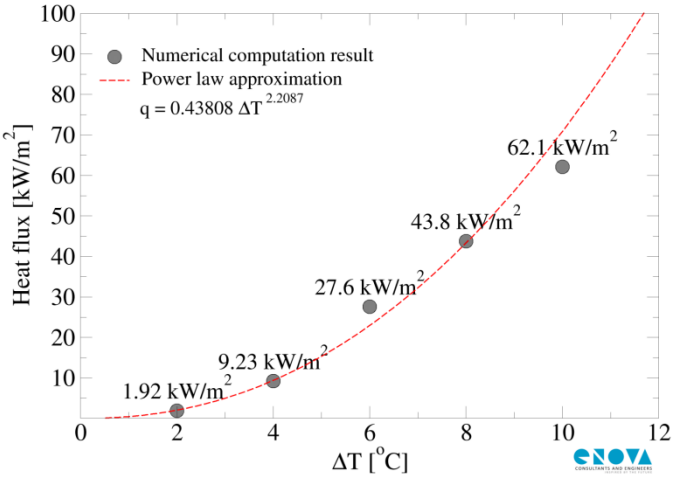

Figure 13. Average heat flux at the heat exchanger surface for different ΔT values after 5 days of computation, along with the power law approximation

VI Conclusion

This study presents a comprehensive analysis of heat transfer phenomena within an aquifer thermal energy storage chamber using Computational Fluid Dynamics (CFD) simulations. Three scenarios are explored: heat transfer due to hot water influx, natural cooling following the closure of inlets/outlets, and heat extraction via a heat exchanger.

Steady-state conditions and stable thermal stratification are observed in all scenarios, with temperature profiles varying depending on the presence of heat sources and sinks, as well as flow patterns. Buoyancy effects are crucial in determining these flow patterns and temperature distributions, especially in scenarios involving hot water influx and natural cooling.

In Scenario A, the average water temperature in the chamber stabilizes at 67.4°C after approximately 20 days. At this point, the heat flux reaches around 65 W/m². The total heat losses for the current chamber amount to 587.6 kW, or 4.8% of the power supplied to the chamber.

In Scenario B, which involves the natural cooling of the water in the chamber, the average temperature decreases from 67.4°C to 55.3°C over 41 days of computation, resulting in an average cooling rate of 0.295°C per day. However, the cooling rate is not linear due to the nature of the heat transfer process. An exponential function accurately predicts the cooling rate, suggesting that the water temperature will reach 30°C in approximately 274 days.

In Scenario C, which focuses on heat extraction using a heat exchanger, the efficiency of heat extraction is influenced by the temperature difference between the heat exchanger surface and the chamber water. Higher temperature differences result in greater heat flux values. Although larger temperature differences allow for more energy extraction, the relationship between

temperature difference and extracted energy is nonlinear, following a power-law dependence rather than a linear trend.

Mathematical models, such as exponential functions and power laws, are proposed to predict temperature variations and heat flux values. These models provide valuable insights into long-term temperature trends and the efficiency of energy extraction.

Numerical simulations based on Computational Fluid Dynamics (CFD) are essential for the accurate prediction of flow and heat transfer phenomena in solid-fluid interactions. These simulations provide detailed insights into the complex behaviour of fluids and thermal fields that are difficult to capture through traditional analytical methods. CFD allows for the modelling of intricate flow patterns, temperature distributions, and the interaction between fluids and solid surfaces, enabling the precise calculation of critical parameters such as heat flux.

The ability to simulate various scenarios, including heat influx, natural cooling, and heat extraction, further highlights the importance of CFD in optimizing system design and improving energy efficiency. Accurate heat flux predictions, for example, are crucial for assessing energy extraction efficiency and ensuring effective thermal management in real-world applications such as aquifer, geothermal systems, and industrial heat exchangers. Therefore, CFD simulations serve as an invaluable tool for advancing the understanding and optimization of heat transfer processes in complex solid-fluid systems.

REFERENCES

[1] Kim, .J, Lee, Y., Yoon, W.S., Jeon, J.S., Koo, M.H., Keehm, Y. Numerical modeling of aquifer thermal energy storage system, Energy, Vol. 35, No. 12, pp. 4955-4965, 2010. https://doi.org/10.1016/j.energy.2010.08.029

[2] Sommer, W.T., Doornenbal, P.J., Drijver, B.C., Van Gaans, P.F.M., Leusbrock, I., Grotenhuis, J.T.C., Rijnaarts, H.H.M. Thermal performance and heat transport in aquifer thermal energy storage, Hydrogeology Journal, Vol. 22, No. 1. pp. 263-279, 2014. http://doi.org/10.1007/s10040-013-1066-0

[3] Major, M., Poulsen, S.E., Balling, N. A numerical investigation of combined heat storage and extraction in deep geothermal reservoirs, Geothermal Energy, Vol. 6, No. 1, pp. 1–16, 2018. https://doi.org/10.1186/s40517-018-0089-0

[4] Schmidt, T., Pauschinger, T., Sørensen, P.A., Snijders, A., Djebbar, R., Boulter, R., Thornton, J. Design aspects for large-scale pit and aquifer thermal energy storage for district heating and cooling, Energy Proc, Vol. 149, pp. 585-594, 2018.https://doi.org/10.1016/j.egypro.2018.08.223

[5] Wesselink, M., Liu, W., Koornneef, J., Van Den Broek, M. Conceptual market potential framework of high temperature aquifer thermal energy storage - A case study in The Netherlands, Energy, Vol. 147, pp. 477-489, 2018. https://doi.org/10.1016/j.energy.2018.01.072

[6] Lee, K.S. A review on concepts, applications, and models of aquifer thermal energy storage systems, Energies, Vol. 3, No. 6, pp. 320-334, 2010. https://doi.org/10.3390/en3061320

[7] Kong, L., Zhu, N. CFD simulations of thermal stratification heat storage water tank with an inside cylinder with openings, Procedia Engineering, Vol. 146, pp. 394-399, 2016. https://doi.org/10.1016/j.proeng.2016.06.419

[8] Feng, H., Li, H., He, S., Qi, J., Han, K., Gao, M. Numerical simulation on thermal stratification performance in thermocline water storage tank with multi-stage middle perforated obstacles, Thermal Science and Engineering Progress, Vol. 35, 101473, 2022. https://doi.org/10.1016/j.tsep.2022.101473

[9] Yaïci, W., Ghorab, M., Entchev, E., Hayden, S. Three-dimensional unsteady CFD simulations of a thermal storage tank performance for optimum design, Applied Thermal Engineering, Vol. 60, No. 1-2, pp. 152-163, 2013. https://doi.org/10.1016/j.applthermaleng.2013.07.001

[10] Gao, L., Lu, H., Sun, B., Che, D., Dong, L. Numerical and experimental investigation on thermal stratification characteristics affected by the baffle plate in thermal storage tank, Journal of Energy Storage, Vol. 34, 102117, 2021. https://doi.org/10.1016/j.est.2020.102117

[11] Hanjalic, K., Popovac, M., Hadziabdic, M. A robust near-wall elliptic-relaxation eddy-viscosity turbulence model for CFD, International Journal of Heat and Fluid Flow, Vol. 25, pp. 1047-1051, 2004. https://doi.org/10.1016/j.ijheatfluidflow.2004.07.005

[12] Hadziabdic, M., Hafizovic, M., Niceno, B., Hanjalic, K. A rational hybrid RANS-LES model for CFD predictions of microclimate and environmental quality in real urban structures, Building and Environment, Vol. 217, 109042, 2022. https://doi.org/10.1016/j.buildenv.2022.109042

[13] Hadziabdic, M., Hodza, A., Niceno, B. Modelling urban canopy with object-based porosity model, International Journal of Heat and Fluid Flow, Vol. 107, 109394, 2024. https://doi.org/10.1016/j.ijheatfluidflow.2024.109394

[14] Hadziabdic, M., Niceno, B. Reconstruction of Nusselt number in RANS computations with wall function approach, Nuclear Engineering and Design, Vol. 412, 112461, 2023. https://doi.org/10.1016/j.nucengdes.2023.112461

[15] Hadziabdic, M. *LES, RANS and Combined Simulation of Impinging Flows and Heat Transfer*, PhD thesis, Delft University of Technology, Delft, The Netherlands, 2006. https://resolver.tudelft.nl/uuid:47cb00a2-d935-4a0a-b68b-a0440cfb9d26 [pristupljeno 24.03.2025]

[16] Hanjalić, K., Laurence, D., Popovac, M., Uribe, J. $v2/k - f$ Turbulence model and its application to forced and natural convection. In: Rodi, W., Mulas, M. (Eds.), *Engineering Turbulence Modelling and Experiments*, Vol. 6, pp. 67-76, 2005. https://doi.org/10.1016/b978-008044544-1/50005-4

[17] Delibra, G., Hanjalic, K., Borello, D., Rispoli, F. Vortex structures and heat transfer in a wall bounded pin matrix: LES with a RANS wall treatment, International Journal of Heat and Fluid Flow, Vol. 31, No. 5, pp. 740-753, 2010. https://doi.org/10.1016/j.ijheatfluidflow.2010.03.004

[18] Wieringa, J. Updating the Davenport roughness classification, Journal of Wind Engineering and Industrial Aerodynamics, Vol. 41, No. 1-3, pp. 357-368, 1992.https://doi.org/10.1016/0167-6105(92)90434-C

[19] Niceno, B. *An Unstructured Parallel Algorithm for Large Eddy and Conjugate Heat Transfer Simulations*, PhD thesis, Delft University of Technology, Delft, the Netherlands, 2001. https://scispace.com/pdf/an-unstructured-parallel-algorithm-for-large-eddy- and-3utpih4hqz.pdf [pristupljeno 23.03.2025]

[20] Niceno, B., Hanjalic, K. Unstructured large-eddy and conjugate heat transfer simulations of wall-bounded flows, in: S. Sunden, M. Faghri (Eds.), *Modelling and Simulation of Turbulent Heat Transfer*, WIT Press, USA, pp. 35-76, 2005.

[21] Borello, D., Salvagni, A., Hanjalic, K. Effects of rotation on flow in an asymmetric rib-roughened duct: LES study, International Journal of Heat and Fluid Flow, Vol. 55, pp. 104-119, 2015. https://doi.org/10.1016/j.ijheatfluidflow.2015.07.012

[22] Palkin, E., Hadziabdic, M., Mullyadzhanov, R., Hanjalic, K. Control of flow around a cylinder by rotary oscillations at a high subcritical Reynolds number, Journal of Fluid Mechanics, Vol. 855, pp. 236-266, 2018. https://doi.org/10.1017/jfm.2018.639

[23] Van Reeuwijk, M., Hadziabdic, M. Modelling high Schmidt number turbulent mass transfer, International Journal of Heat and Fluid Flow, Vol. 51, pp. 42-49, 2015. https://doi.org/10.1016/j.ijheatfluidflow.2014.10.025

[24] Temmerman, L., Hadziabdic, M., Leschziner, M.A., Hanjalic, K. A hybrid two-layer URANS–LES approach for large eddy simulation at high Reynolds numbers, International Journal of Heat and Fluid Flow, Vol. 26, No. 2, pp. 173-190, 2005. https://doi.org/10.1016/j.ijheatfluidflow.2004.07.006

[25] Hafizovic, M., Hadziabdic, M., Niceno, B. Simulation of pollutant dispersion in a real urban configuration under strong stratification, in Proc. *10th International Symposium on Turbulence, Heat and Mass Transfer, THMT-23*, Rome, Italy, pp. 12, 11-15 September 2023. http://dx.doi.org/10.1615/ICHMT.THMT-23.820

AUTHORS

Mahir Hafizović – MSc., Senior Assistant, Enova d.o.o./International University of Sarajevo – Mechanical Eng. Department, mahir.hafizovic@enova.ba, ORCID 0000-0002-9319-6932

Muhamed Hadžiabdić – Prof. Dr., International University of Sarajevo – Mechanical Eng. Department, mhadziabdic@ius.edu.ba, ORCID 0000-0002-2726-3914

Bojan Ničeno – Dr., Senior Scientist, Paul Scherrer Institute – Nuclear Energy and Safety Department, bojan.niceno@psi.ch, ORCID 0000-0002-8583-1684

Numeričke simulacije prenosa toplote u sistemu podzemnog skladištenja termalne energije (UTES): CFD pristup

Rezime **-** Fenomen prenosa toplote unutar podzemnog skladišta toplotne energije analiziran je koristeći metodu računske dinamike fluida (CFD). Analizirana su tri scenarija kako bi se istražili mehanizmi prenosa toplote: (i) *Dotok tople vode* – Topla voda ulazi u komoru, potiskuje hladniju vodu i prenosi toplotu na okolno tlo i odlaznu vodu. Tlo, kao toplotni rezervoar, apsorbuje toplotu uz minimalne promjene temperature, osim u blizini komore; (ii) *Prirodno hlađenje* – Kada su ulazi i izlazi zatvoreni, voda se postepeno hladi kroz interakciju s hladnijim tlom. Posebno je analizirana početna brzina hlađenja, koja određuje koliko dugo voda ostaje iznad određene temperature prije nego što sistem dostigne termičku ravnotežu; (iii) *Ekstrakcija toplote izmjenjivačem* – Uronjeni izmjenjivač odvodi toplotu iz vode u komori, dok okolno tlo nadoknađuje gubitak. Efikasnost ovog procesa zavisi od dimenzija i radnih parametara izmjenjivača.

Rezultati pokazuju da sistem u svim scenarijima zadržava stabilnu termičku stratifikaciju, gdje toplija voda ostaje u gornjim slojevima, dok se hladnija spušta uslijed razlika u gustini. Interakcija vode i tla je ključna – tlo djeluje kao izvor toplote tokom ekstrakcije i kao rezervoar tokom hlađenja..

Ključne reči **-** Skladištenje toplotne energije, prenos toplote, geotermalna energija, interakcija čvrstog tijela i fluida, akvifer, računska dinamika fluida (CFD)